Electronic thermal conductivity and thermoelectric figure of merit of *n*-type PbTe/$Pb_{1-x}Eu_xTe$ quantum wells

I. Sur* and A. Casian
Department of Informatics, Computers and Microelectronics, Technical University of Moldova, MD-2004 Chişinău, Moldova

A. Balandin
Nano-Device Laboratory, Department of Electrical Engineering, University of California-Riverside, Riverside, California 92521, USA
(Received 29 May 2003; revised manuscript received 22 September 2003; published 12 January 2004)

We have investigated the electronic thermal conductivity and thermoelectric figure of merit of (100) and (111) oriented PbTe/$Pb_{1-x}Eu_xTe$ quantum wells. Our theoretical formalism includes the nonparabolicity of the carrier dispersion, band anisotropy, as well as carrier scattering on acoustic and optical phonons and presents a substantial improvement over existing models. The kinetic equations are solved by iterations taking into account multisubband transitions. The values of the electronic thermal conductivity and thermoelectric figure of merit are examined in a wide range of the quantum well widths and carrier concentrations. It is found that in (111) oriented quantum wells the electronic thermal conductivity and Lorentz number are strongly enhanced due to the lifting of the valley degeneracy. The effect of the confined carrier-phonon scattering on the value of the thermoelectric figure of merit is analyzed in detail. The obtained results are in good agreement with available experimental data for thin quantum wells and bulk material. The developed formalism can be used for accurate simulation of the thermoelectric properties of low-dimensional structures.

DOI: 10.1103/PhysRevB.69.035306 PACS number(s): 73.63.Hs, 72.20.Pa

I. INTRODUCTION

The field of thermoelectrics has witnessed a strong renewal of interest about a decade ago with the proposals to improve the thermoelectric properties of some materials by preparing them in the form of quantum well (QW) two-dimensional (2D) multilayered structures[1,2] or one-dimensional (1D) quantum wire array structures.[3] A significant enhancement of the thermoelectric power factor and two-dimensional thermoelectric figure of merit $Z_{2D}T$ has been predicted for QW's due to the increased carrier density of states per unit volume as compared to bulk thermoelectrics.[1–3] In these papers the simplest models of the quantum wells with an infinite barrier potential and constant relaxation time approximation for carrier transport have been used. In the later papers[4–6] the theoretical description of quantum wells has been made more rigorous. Several types of QW structures were considered in different temperature intervals. The general conclusion was that the *ZT* enhancement in quantum wells is not as drastic as predicted by the original simple models. At the same time an alternative way of achieving higher *ZT* via the decrease of the in-plane phonon thermal conductivity in low-dimensional structures such as quantum wells or quantum wires has been proposed.[7] It is based on the idea of acoustic phonon spectrum modification in low-dimensional structures embedded to material of distinctively different elastic properties.[7]

More recently, attention turned to structures of even lower dimensionality such as quantum dot arrays.[8,9] In quantum dot arrays and superlattices the improvement of the thermoelectric characteristics is expected to come from carrier miniband formation and reduction of the phonon thermal conductivity. A decrease of thermal conductivity is possible due to the increased phonon-boundary scattering at the interfaces, as well as, due to the change in the phonon dispersion. A controlled modification of phonon modes to achieve lower thermal conductivity or carrier-phonon scattering rate suppression has been termed the phonon engineering.[10]

The first experimental investigation of PbTe/$Pb_{1-x}Eu_xTe$ quantum wells has shown[11,12] a significant increase of power factor and *ZT* in individual conduction layers. These results have stimulated further theoretical[13–17] and experimental[18–21] research. The quantitative treatment[14] of the thermoelectric power in thin QW's has demonstrated a good agreement between theoretical and experimental results. The power factor and figure of merit have been calculated in Refs. 13 and 15–17. However, quantitatively the values obtained on the basis of the various proposed models show significant discrepancy. Therefore, a more rigorous and complete theoretical analysis of the thermoelectric properties of QW's becomes an important and timely problem.

In this paper we present a very detailed and comprehensive investigation of the thermoelectric properties of *n*-type PbTe/$Pb_{1-x}Eu_xTe$ QW's. First, we consider the effect of energy band nonparabolicity on the thermoelectric characteristic. This is done on the basis of QW model,[15] which allows to take into account the anisotropy of effective masses, the multivalley character of the constituent bulk materials, the dependence of the effective masses on the quantum well height and width, the presence or absence of the valley degeneracy, the effect of carrier penetration into barriers, and the coupling between longitudinal motion of electrons along the well and transversal motion across the well. The quantum well material, PbTe, belongs to the narrow-gap semiconductors, and, therefore, the effect of energy band nonparabolicity can be very important. Recently, it has been demonstrated that the nonparabolicity plays a significant role in determining the value of the thermoelectric power.[14] As second task, we investigate the electronic thermal conductivity of quantum wells, which has not been done before. The electronic contribution is important and has to be included in consideration because the optimal QW parameters are achieved at a

higher carrier concentration than that in bulk materials. Moreover, the Lorentz number, as will be shown, increases and the contribution of electrons to the total thermal conductivity can be very high. In addition, we take into account the recent reevaluation of the $Pb_{1-x}Eu_xTe$ band parameters[22] and barrier potential height.[14] The electronic thermal conductivity, Lorentz number, and thermoelectric figure of merit are calculated for the in-plane QW transport as the functions of the quantum well width and carrier concentration. Our model includes the scattering on both acoustical and optical phonons. It is general enough to allow for the carrier intersubband transitions to be taken into consideration. The kinetic equations are solved by the iterative method. The investigation is focused on structures of (100) and (111) crystallographic orientation. The maximum expected value of the thermoelectric figure of merit and the optimal structural parameters required to achieve it are determined. Our results are then compared with those obtained on the basis of other very distinct theoretical models and available experimental data.

II. GENERAL CONSIDERATION

Let us consider the carrier transport along $PbTe/Pb_{1-x}Eu_xTe$ QW in the presence of a weak electric field $\mathbf{E}$ and a temperature gradient ∇T, which are parallel to each other. The electrical $\mathbf{I}_e$ and thermal $\mathbf{I}_q$ currents densities are related with the field and temperature gradient as

$$\mathbf{I}_e=\hat{\sigma}\mathbf{E}-(\widehat{\sigma S})\nabla T, \quad \mathbf{I}_q=T(\widehat{\sigma S})\mathbf{E}-\hat{\gamma}\nabla T, \tag{1}$$

where $\hat{\sigma},\hat{S},\hat{\gamma}$ are the tensors of electrical conductivity, Seebeck coefficient, and electronic thermal conductivity, respectively. The later is determined at zero electric field. The usual thermal conductivity at zero electric current $\hat{k}^e$ is given by $\hat{k}^e=\hat{\gamma}-T(\widehat{\sigma S})\hat{S}$. The current densities (1) can be calculated using

$$\mathbf{I}_e=\frac{2e}{V}\sum_{a,\nu}\mathbf{V}_a^\nu f_a^\nu, \quad \mathbf{I}_q=\frac{2}{V}\sum_{a,\nu}(E_a^\nu-\mu)\mathbf{V}_a^\nu f_a^\nu, \tag{2}$$

where f_a^ν is the nonequilibrium distribution function, E_a^ν and $\mathbf{V}_a^\nu$ are the full energy and the velocity of an electron, a is the set of quantum numbers of electronic states in the ν valley, μ is the chemical potential, and e is the electron charge. The currents are sums of currents from different valleys ν, and $\hat{\sigma}$, $(\widehat{\sigma S})$, $\hat{\gamma}$ are the sums of corresponding contributions from each valley, too.

To describe the electronic states in the given valley, we have used the Hamiltonian[23] that takes into account in the simplest approximation the nonparabolicity of the carrier dispersion law,

$$H=-\frac{\hbar^2}{2}\sum_{ij}\frac{\partial}{\partial x_i}\left(\frac{1}{m(z,E)}\right)_{ij}\frac{\partial}{\partial x_j}+U(z).$$

$$x_i=(x,y,z). \tag{3}$$

Here x,y are in-plane axes, and z is perpendicular to the well plane, $U(z)$ is the confinement potential of the QW, $U(z)=U$, when $|z|>d/2$ and $U(z)=0$, when $|z|<d/2$, where U is the conduction-band offset between the well and the barrier material, and d is the QW width. The components of the inverse effective masses tensor m_{ij}^{-1} receive their barrier values for $|z|>d/2$ and the well ones for $|z|<d/2$. In the local coordinate system, connected with the main axes of νth ellipsoid of constant energy, the tensor m_{ij}^{-1} is diagonal and its components are given by[23]

$$m_{\parallel,\perp}^W(E)=m_{\parallel,\perp}^W(1+E/E_g^W),$$

$$m_{\parallel,\perp}^B(E)=m_{\parallel,\perp}^B[1+(E-U)/E_g^B],$$

where $m_\parallel^{W,B}$ are the longitudinal and $m_\perp^{W,B}$ the transversal band-edge effective masses in the well and in the barrier, respectively, E is the electron energy, which is determined from the Schrödinger equation with the Hamiltonian (3), $E_g^{W,B}$ are the band gaps of the well and of the barrier materials. Solving the Schrödinger equation in all three regions of the structure and using the Bastard[24] boundary conditions at interfaces, one can obtain

$$p(E,\mathbf{k})=\alpha\pi-2\arcsin[r(E,\mathbf{k})],$$

$$p(E,\mathbf{k})=\left\{\frac{2m_z^W(E)d^2}{\hbar^2}[E-\varepsilon^W(\mathbf{k})]\right\}^{1/2},$$

$$r(E,\mathbf{k})=\left\{\frac{E-\varepsilon^W(\mathbf{k})}{\frac{m_z^W(E)}{m_z^B(E)}[U+\varepsilon^B(\mathbf{k})-E]+E-\varepsilon^W(\mathbf{k})}\right\}^{1/2}. \tag{4}$$

Here $m_z^{W,Z}(E)$ are the z components[25] of electron effective masses in the well and in the barrier, $\varepsilon^{W,B}(\mathbf{k})$ has the structure of electron kinetic energy, calculated with the masses, which depend on E, $\mathbf{k}$ is the 2D electron wave vector, $\mathbf{k}=(k_x,k_y)$. The solution of Eq. (4) gives the electron dispersion law in the αth subband: $E_{\mathbf{k}\alpha}=E_\alpha+\mathcal{E}_{\mathbf{k},\alpha}$, where E_α is the energy of dimensional quantization, $\mathcal{E}_{\mathbf{k},\alpha}$ is the kinetic energy in the αth subband. Equation (4) was solved numerically. The following material parameters[22,26] are used in simulations: $m_\parallel^W=0.35m_0$, $m_\perp^W=0.034m_0$, $E_g^W=321$ meV for PbTe and $m_\parallel^B=0.495m_0$, $m_\perp^B=0.049m_0$, $E_g^B=635$ meV for barrier material with $x=0.09$ ($U=173$ meV) at $T=300$ K. We consider QW's with (100) and (111) orientation. In the case of (100) orientation all four ellipsoids of constant energy of the bulk PbTe are equivalent and the energy subbands in them coincide. In the case of (111) oriented QW the valley degeneracy is partially lifted. Two sets of subbands arising from different valleys appear. One set is from longitudinal ellipsoid perpendicular to QW and is situated below the second one from the oblique ellipsoids. Substituting $k=0$ into Eq. (4) we found the energies E_α of dimensional quantization as functions of the well width d. With increasing d the number of levels in QW increases. New levels appear at equal intervals of d as in the parabolic model, but at $d_\alpha^*=\hbar\pi(\alpha-1)/[2m_z^WU\,(1+U/E_g^W)]^{1/2}$. In Fig. 1 we showed the dependencies of the dimensional quan-

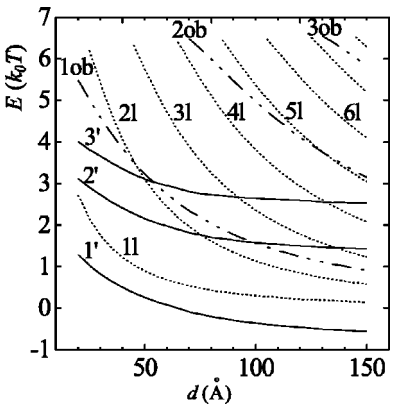

FIG. 1. Quantum-well energy levels and Fermi levels expressed in k_0T units as a function of the well width d for (111) oriented PbTe/$Pb_{1-x}Eu_xTe$ well. Curves 1l to 8l denote the levels $E_{1l},E_{2l},\ldots,E_{8l}$, arising from the longitudinal ellipsoid along the [111] direction, curves $1ob$ to $3ob$ denote the levels E_{1ob}, E_{2ob}, and E_{3ob} arising from the oblique to [111] direction ellipsoids. Curves $1'$, $2'$, and $3'$ correspond to Fermi level: $1'$ is for $n=10^{18}$ cm^{-3}, $2'$ is for $n=5\times10^{18}$ cm^{-3}, $3'$ is for $n=10^{19}$ cm^{-3}.

tization energies on well width d for (111) QW. Qualitatively, the dependencies of all energies on well width, including Fermi energy, are similar to those of Ref. 15, where we have used the parabolic approximation and more heavier effective masses. But now their values are higher by $0.5-1k_0T$.

Besides, the dispersion law $\mathcal{E}_{\mathbf{k}\alpha}$ becomes nonparabolic. Numerical investigation of Eq. (4) has shown that with a good precision $\mathcal{E}_{\mathbf{k}\alpha}$ can be approximated by a Kane-like dispersion law,

$$\mathcal{E}_{\mathbf{k}\alpha}=(E_{g\alpha}/2)\{[1+4\eta_{\mathbf{k}\alpha}/E_{g\alpha}]^{1/2}-1\},$$

$$\eta_{\mathbf{k}\alpha}=\hbar^2k_x^2/2m_{x\alpha}+\hbar^2k_y^2/2m_{y\alpha}, \tag{5}$$

where

$$m_{i\alpha}^{-1}=\left(\frac{1}{m_i^W(E_\alpha)}(1+y_\alpha)+\frac{1}{m_i^B(E_\alpha)}\frac{E_\alpha}{U-E_\alpha}\right)\times\left(2y_\alpha+\frac{m_z^W(0)}{m_z^W(E_\alpha)}(1-y_\alpha)+\frac{m_z^B(U)}{m_z^B(E_\alpha)}\frac{E_\alpha}{U-E_\alpha}\right)^{-1},$$

$$y_\alpha=p(E_\alpha,0)\{2r_0(1-r_0^2)^{1/2}\}^{-1},\quad i=(x,y), \tag{6}$$

and $r_0=r[E_\alpha,0,m_z^W(0),m_z^B(U)]$, x,y are parallel to the main axes of the ellipse of constant energy $\eta_{\mathbf{k}\alpha}$, $E_{g\alpha}=E_g^W+E_\alpha$. At small values of $\eta_{\mathbf{k}\alpha}$ the approximate expression (5) coincides with the exact one and is close to the parabolic $\mathcal{E}_{\mathbf{k}\alpha}\approx\eta_{\mathbf{k}\alpha}$ with new effective masses, given by Eq. (6). At large $\eta_{\mathbf{k}\alpha}$ the dispersion law becomes linear and the values of $\mathcal{E}_{\mathbf{k}\alpha}$ given by Eq. (5) are smaller than the exact solution obtained from Eq. (4) numerically, by not more than 5%. The masses determined by Eq. (6) depend on the energy of dimensional quantization and on the potential height U. For small E_α, when levels are close to the bottom of the quantum well, $m_{i\alpha}$ take the values of masses m_i^W in the QW. With the increase of E_α the effective masses increase mainly as a result of the effect of nonparabolicity[27] and partially due to the penetration of the wave function into the barrier.[15] For E_α close to U the second of the mentioned effects becomes more important and the effective masses take the values of carrier masses m_i^B into barriers. The numerical study of Eq. (6) has also shown that with a high precision the masses of electrons from different subbands α and β are connected by the relation $m_{x\alpha}/m_{y\alpha}\approx m_{x\beta}/m_{y\beta}$, i.e., all curves of constant energy $\mathcal{E}_{\mathbf{k}\alpha}$ for a given QW have similar forms.

To calculate the kinetic coefficients we used the expressions (1) and (2) and the Boltzmann equation approach for the determination of the distribution function. The elastic carrier scattering on deformation acoustic (DA) bulk phonons and the inelastic one on bulk longitudinal optical (LO) phonons were considered. Usually, in such situations the variational method or the iterative method are applied for solving the kinetic equation. The thermal conductivity is expressed through the second moment of the function of energy[28] connected with $f_{\mathbf{k}\alpha}$ and one can expect that its value is more sensitive to the form of $f_{\mathbf{k}\alpha}$, than the conductivity, which is expressed through the zero moment. Therefore, we used the iterative method,[29] which gives more exact numerical solution of the kinetic equation. To take into account the mass anisotropy all vectors have been subjected to the transformation $\mathbf{k}^*=\hat{g}_\alpha\mathbf{k}$, $\mathbf{V}_{\mathbf{k}\alpha}^*=\hat{g}_\alpha^{-1}\mathbf{V}_{\mathbf{k}\alpha}$, $\mathbf{E}^*=\hat{g}_\alpha\mathbf{E}$, $\nabla T^*=\hat{g}_\alpha\nabla T$, $g_{\alpha ij}=g_{\alpha i}\delta_{ij}$, $g_{\alpha x}=1$, and $g_{\alpha y}=(m_{x\alpha}/m_{y\alpha})^{1/2}$, $\eta_{\mathbf{k}^*\alpha}=\hbar^2k^{*2}/2m_{x\alpha}$, $\eta_{\mathbf{k}^*\beta}=(m_{x\alpha}/m_{x\beta})\eta_{\mathbf{k}^*\alpha}$ (further we shall omit the sign* over new vectors). In this coordinate system the linearized Boltzmann equations are

$$-e(\mathbf{V}_{\mathbf{k}\alpha}\mathbf{E})+\frac{E_{\mathbf{k}\alpha}-\mu}{T}(\mathbf{V}_{\mathbf{k}\alpha}\nabla T)=\frac{2\pi}{\hbar}g_{\alpha y}^{-1}\sum_{\mathbf{Q}\beta}A_{\mathbf{Q}}^2|I_{\alpha\beta}(\mathbf{Q})|^2(\Phi_{\mathbf{k}-\mathbf{q},\beta}-\Phi_{\mathbf{k}\alpha})\frac{n_{\mathbf{k}-\mathbf{q},\beta}}{n_{\mathbf{k}\alpha}}\times\{N(\omega_{\mathbf{Q}})\delta^+ +[N(\omega_{\mathbf{Q}})+1]\delta^-\},$$

$$f_{\mathbf{k}\alpha}=n_{\mathbf{k}\alpha}+\frac{1}{k_0T}n_{\mathbf{k}\alpha}(1-n_{\mathbf{k}\alpha})\Phi_{\mathbf{k}\alpha},$$

$$\delta^\pm=\delta(\pm\hbar\omega_{\mathbf{Q}}-E_{\mathbf{k}\alpha}+E_{\mathbf{k}-\mathbf{q},\beta}). \tag{7}$$

Here $A_{\mathbf{Q}}$ is the electron-phonon matrix element and in nontransformed coordinate system $A_{\mathbf{Q}}^2=2\pi e^2\chi\hbar\omega_0/VQ^2$, $\chi=\varepsilon_\infty^{-1}-\varepsilon_0^{-1}$, $\omega_{\mathbf{Q}}=\omega_0$ for interaction with longitudinal optical phonons, $A_{\mathbf{Q}}^2=\hbar E_1^2Q/2V\rho s$, for deformation acoustic phonons, $\omega_{\mathbf{Q}}$ and N are the phonon frequency and phonon distribution function, $\mathbf{Q}$ is the 3D phonon wave vector, $\mathbf{Q}=(\mathbf{q},q_z)$, V is the system volume, E_1 is the deformation potential constant, s is the sound velocity, ρ is the mass density, ε_0 and ε_∞ are the static and high-frequency dielectric constants, $n_{\mathbf{k}\alpha}$ is the equilibrium Fermi-Dirac distribution function, $\mathbf{V}_{\mathbf{k}\alpha}=\hbar^{-1}\nabla_{\mathbf{k}}\mathcal{E}_{k\alpha}$ is the electron velocity. For small content of Eu in barriers and QW's larger than 20 Å considered here, the phonon confinement can be neglected and phonons are considered as in bulk PbTe. The scattering form factor $I_{\alpha\beta}(\mathbf{Q})$ is given in Ref. 15. The intervalley scattering was neglected as less important at room temperature. The new function $\Phi_{\mathbf{k}\alpha}$, which characterizes the deflection of nonequilibrium distribution function from $n_{\mathbf{k}\alpha}$, is searched

in the form[30] $\Phi_{\mathbf{k}\alpha}=V_{\mathbf{k}\alpha}\,[e(\boldsymbol{\tau}^{E}_{\mathbf{k}\alpha}\mathbf{E})-(\boldsymbol{\tau}^{T}_{\mathbf{k}\alpha}\boldsymbol{\nabla}k_0T)]$. In the quasielastic scattering approximation $\boldsymbol{\tau}^{E}_{\mathbf{k}\alpha}$ has the meaning of the relaxation time vector for electrical processes. In this approximation the scattering function $\boldsymbol{\tau}^{T}_{\mathbf{k}\alpha}$ is related with $\boldsymbol{\tau}^{E}_{\mathbf{k}\alpha}$ as $\boldsymbol{\tau}^{T}_{\mathbf{k}\alpha}=[(E_{\mathbf{k}\alpha}-\mu)/k_0T)]\,\boldsymbol{\tau}^{E}_{\mathbf{k}\alpha}$. Taking into account the symmetry of Eq. (7), we have decomposed the angular dependencies of $\boldsymbol{\tau}^{E(T)}_{\mathbf{k}\alpha}$ into Fourier series,[30] and have kept the first nonvanishing terms. Then $\Phi_{\mathbf{k}\alpha}=\Sigma_i V_{\mathbf{k}\alpha i}\,[e\tau^{E}_{\alpha i}(\varepsilon)E_i-\tau^{T}_{\alpha i}(\varepsilon)(\boldsymbol{\nabla}k_0T)_i]$, where ε is the kinetic energy of an electron in α th subband. The inverse Fourier transformation of Eq. (7) gives the system of coupled equations

$$\tau^{E(T)}_{\alpha i}(\varepsilon)=\left\{\xi^{E(T)}_{\alpha}+\sum_{\beta}\,[\tau^{E(T)}_{\beta i}(\varepsilon^{-}_{\alpha\beta})S^{-}_{\alpha\beta i}+\tau^{E(T)}_{\beta i}(\varepsilon^{+}_{\alpha\beta})S^{+}_{\alpha\beta i}]\right\}\Big/\,S^{0}_{\alpha i}. \tag{8}$$

Here $\varepsilon^{\pm}_{\alpha\beta}=\varepsilon+E_\alpha-E_\beta\pm\hbar\omega_0$, $\xi^{E}_{\alpha}=1$, $\xi^{T}_{\alpha}=(\varepsilon+E_\alpha-\mu)/k_0T$, and

$$S^{\pm}_{\alpha\beta i}=\frac{2\pi}{\hbar}\,\frac{2}{\pi}\int_0^{\pi}d\vartheta\,\frac{k_i}{k}\,g^{-1}_{\alpha y}\sum_{\mathbf{Q}}\,A^{2}_{\mathbf{Q}}|I_{\alpha\beta}(\mathbf{Q})|^{2}\frac{n_{\mathbf{k}-\mathbf{q},\beta}}{n_{\mathbf{k}\alpha}}\times\frac{V_{\mathbf{k}-\mathbf{q},\beta,i}}{V_{\mathbf{k},\alpha}}\left(N+\frac{1}{2}\pm\frac{1}{2}\right)\delta^{\mp}, \tag{9}$$

$$S^{0}_{\alpha i}=\frac{2\pi}{\hbar}\,\frac{2}{\pi}\int_0^{\pi}d\vartheta\left(\frac{k_i}{k}\right)^{2}g^{-1}_{\alpha y}\sum_{\mathbf{Q}\beta}\,A^{2}_{\mathbf{Q}}|I_{\alpha\beta}(\mathbf{Q})|^{2}\frac{n_{\mathbf{k}-\mathbf{q},\beta}}{n_{\mathbf{k}\alpha}}\times[N\delta^{+}+(N+1)\,\delta^{-}], \tag{10}$$

ϑ is the angle between $\mathbf{k}$ and x axis. In the case of carrier scattering on LO and DA phonons it is necessary to add to $S^{0}_{\alpha i}$ the acoustic contribution

$$S^{0,ac}_{\alpha i}=(\tau^{ac}_{\alpha})^{-1}=\frac{E_1^{2}k_0T}{\hbar^{3}\rho s^{2}}(m_{x\alpha}m_{y\alpha})^{1/2}\times\sum_{\beta}\,\frac{m_{x\beta}}{m_{x\alpha}}\Gamma_{\alpha\beta}I_{\alpha\beta}\theta(\varepsilon+E_\alpha-E_\beta), \tag{11}$$

$$\Gamma_{\alpha\beta}=[1+4(\varepsilon+E_a-E_\beta)(\varepsilon+E_\alpha-E_\beta+E_{g\beta})/E^{2}_{g\beta}]^{1/2}, \tag{12}$$

$$I_{\alpha\beta}=\int dz|\varsigma_\alpha(z)|^{2}|\varsigma_\beta(z)|^{2}. \tag{13}$$

τ^{ac}_{α} is the relaxation time of electrons in α subband, θ is the Heaviside step function, $\varsigma_\alpha(z)$ is the normalized electron wave function in z direction. The scattering on acoustic phonons in the elastic approximation is isotropic, the factor $A^{2}_{\mathbf{Q}}N(\omega_{\mathbf{Q}})$ in Eq. (7), where $\omega_Q=sQ$, does not depend on $\mathbf{Q}$. As a result, the relaxation times are isotropic too: $\tau^{ac}_{\alpha x}=\tau^{ac}_{\alpha y}=\tau^{ac}_{\alpha}$. The dependence $\tau^{ac}_{\alpha}(\varepsilon)$ has steplike character. At the electron energy $\varepsilon=E_\beta-E_\alpha$, $E_\beta>E_\alpha$, when a new channel of energy relaxation with the carrier transition to higher levels β becomes open, the relaxation time sharply decreases. The values of these steps are determined by the form factor (13) and by the change of the dispersion law after transition. In the intervals between steps the dependence $\tau^{ac}_{\alpha}(\varepsilon)$ is connected with the effect of nonparabolicity.

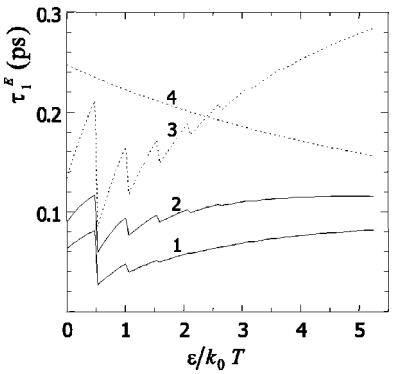

FIG. 2. Relaxation times $\tau^{E}_{1,x}$ (curve 1) and $\tau^{E}_{1,y}$ (curve 2) for x and y direction in oblique valley of (111) oriented QW as a function of electron energy ε. The contributions of scattering on optical (curve 3) and acoustical (curve 4) phonons into $\tau^{E}_{1,y}$ are also shown.

In the case of scattering on LO and DA phonons, the functions $\tau^{E(T)}_{\alpha i}(\varepsilon)$ were found numerically from Eq. (8). The values of parameters were taken from Ref. 31. The relaxation times as a function of carriers energy are shown in Fig. 2 for (111) oriented QW at $T=300$ K, $n=5\times10^{18}$ cm^{-3}, and $d=20$ Å, when all valleys contain one energy subband. The curves $\tau^{E}_{\alpha i}(\varepsilon)$ have, as in the bulk,[32] the form characteristic for the carrier scattering on LO phonons. With increasing ε, the relaxation time increases, too. At the energy $\varepsilon=\hbar\omega_0$ ($\hbar\omega_0=0.526k_0T$, $T=300$ K) the electrons obtain the possibility to radiate a LO phonon and to leave that state. At temperature $k_0T\sim\hbar\omega_0$ the number of phonons is not great and the relaxation time and the distribution function decrease considerably (the first jump in Fig. 2). The minimum of distribution function at $\varepsilon=\hbar\omega_0$ and the presence of term with the argument $\varepsilon^{+}_{\alpha\beta}$ in Eq. (8), which describes the scattering processes from the lower energy state into the given state, provide the appearance of minimums at energies $\varepsilon=m\hbar\omega_0$, $m=2,3,\ldots$.

These minimums become less expressed at high m. At considered carrier densities the electrons with $\varepsilon\sim k_0T$ play the main role in the thermoelectric transport. The comparison of curves 2, 3, 4 shows that at these energies the carrier scattering by LO and DA phonons gives comparable contributions to the formation of distribution function. At higher ε the scattering by acoustic phonons becomes dominant. Note that the relaxation time $\tau^{E}_{\alpha y}(\varepsilon)$ (curve 2) for y direction is greater than $\tau^{E}_{\alpha x}(\varepsilon)$ (curve 1), although the inverse relation takes place for mobility ($m_{y\alpha}>m_{x\alpha}$).

In thin quantum wells, quantitatively close results for relaxation times were obtained for longitudinal subbands of (111) and for oblique ones of (100) oriented QW's in both cases of scattering on acoustic[14] and on optical phonons. Large in plane effective masses correspond to a small mass of dimensional quantization. In thin QW's with finite potential height this leads to the spread of the wave functions $\varsigma_\alpha(z)$ and to diminution of the form factors for scattering on DA and LO phonons. As a result, the relaxation times weakly depend on QW orientation in spite of essential change of effective masses.

Using Eqs. (1), (2), and (8) one can find the transport coefficients. In the coordinate system connected with the main axes of ellipses of constant energy $\eta_{\mathbf{k}\alpha}$, the tensors $\hat{\sigma}$, $(\widehat{\sigma S})$, $\hat{\gamma}$ are diagonal and their components for each valley are

$$\sigma_{ii}=\frac{e^2}{\pi\hbar^2 k_0 T d}L_{i,0}^{E}, \tag{14}$$

$$(\sigma S)_{ii}=\frac{k_0}{e}\frac{e^2}{\pi\hbar^2 k_0 T d}L_{i,0}^{T}=\frac{k_0}{e}\frac{e^2}{\pi\hbar^2 k_0 T d}L_{i,1}^{E}, \tag{15}$$

$$\gamma_{ii}=\left(\frac{k_0}{e}\right)^2\frac{e^2}{\pi\hbar^2 k_0 T d}L_{i,1}^{T}, \tag{16}$$

$$L_{i,n}^{E(T)}=\sum_{\alpha} g_{\alpha y}^{-1} g_{\alpha i}^{2}\int_0^{\infty} d\varepsilon\,\varepsilon\left(1+\frac{\varepsilon}{E_{g\alpha}}\right)\left(\frac{\varepsilon+E_{\alpha}-\mu}{k_0 T}\right)^{n} \times(1+2\varepsilon/E_{g\alpha})^{-1} n_{\mathbf{k}\alpha}(1-n_{\mathbf{k}\alpha})\tau_{\alpha i}^{E(T)}(\varepsilon),\quad n=0,1. \tag{17}$$

To obtain the full transport coefficients, the tensors (14)–(16) deriving from different valleys were led to one definite coordinate system and summarized. It gives, for example, $\sigma_{100}=2(\sigma_{xx}+\sigma_{yy})$ for (100) oriented QW and $\sigma_{111}=\sigma^{l}+3(\sigma_{xx}^{ob}+\sigma_{yy}^{ob})/2$ for (111) QW, where σ^{l} and σ_{ii} are the conductivities of longitudinal (111) and oblique subbands. Due to Onsager symmetry principle, the functions $\tau_{\alpha i}^{E}(\varepsilon)$ and $\tau_{\alpha i}^{T}(\varepsilon)$ are related through Eq. (15), which was used to check up the numerical calculations.

III. RESULTS AND DISCUSSION

Using Eqs. (14)–(17) we have calculated the electronic thermal conductivity k^e, Lorentz number $L=k^e/\sigma T$, and thermoelectric figure of merit $ZT=\sigma S^2 T/(k^{\mathrm{latt}}+k^e)$ of the QW layer, where $k^{\mathrm{latt}}=2$ W/m K is the lattice contribution to the thermal conductivity of PbTe. The electronic thermal conductivity and Lorentz number as a function of well width d are shown in Figs. 3(a) and 3(b), respectively, for (100) and (111) oriented QW's. In the case of (100) QW's the fourfold valley degeneracy is preserved. The curves $k_{100}^{e}(d)$ [Fig. 3(a), curves 1–3] are similar, in general, to the forms of corresponding curves for $\sigma_{100}(d)$. With increasing d the thermal conductivity increases. The Lorentz number [curves 1–3 of Fig. 3(b)] has a more complicated behavior. At small d it is approximately constant. At $d=d_{\alpha}^{*}$ new energy levels E_{α} appear in the QW. Because of small population these levels have a negligible effect on the conductivity. However, due to the great energy, the carriers in these states give more significant contribution to the heat transport and, respectively, k_{100}^{e} and L_{100} a little increase near d_{α}^{*}. With a further increase of the well width, E_{α} quickly decreases, and both k_{100}^{e} and L_{100} diminish too. As a result, small peaks appear on the curves $k_{100}^{e}(d)$ and $L_{100}(d)$ at $d=d_{\alpha}^{*}$. The increase of Lorentz number at $d>80$ Å (curves 2 and 3) is connected mainly with the change of statistics of electrons on the first subband from nondegenerate at small d to a slightly degenerate at greater d. Note that the multisubband carrier transport has a relatively small effect on the Lorentz number L. As in the bulk, the values of L_{100} vary from $L_{100}=2.1(k_0/e)^2$,

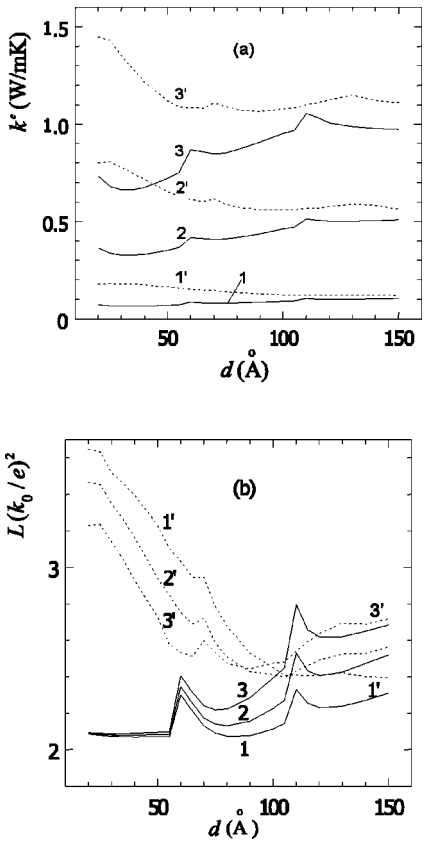

FIG. 3. Calculated electronic thermal conductivity (a) and Lorentz number (b) of PbTe/$Pb_{1-x}Eu_xTe$ quantum well as function of well width d for (100) oriented QW (curves 1, 2, 3) and for (111) ones (curves 1′, 2′, 3′). Curves 1 and 1′ are for $n=10^{18}$ cm^{-3}, 2 and 2′ for $n=5\times10^{18}$ cm^{-3}, 3 and 3′ for $n=10^{19}$ cm^{-3}.

characteristic for the combined carrier scattering on acoustic and optical phonons in the case of Boltzmann statistics and nonparabolic dispersion law up to values, characteristic for the degeneracy beginning.

Curves 1′–3′ in Figs. 3(a) and 3(b) show the dependencies of thermal conductivity and Lorentz number on well width for (111) oriented QW. In this case the confinement partially lifts the valley degeneracy and the carriers become separated into two groups of longitudinal and oblique subbands, respectively, with very different energies. Note that for QW of high symmetric orientations in cubic crystals the relation $m_x m_y m_z=m_{\perp}^2 m_{\parallel}$ is carried out[25] for all equivalent ellipsoids in the bulk. In the oblique ellipsoids m_z^{ob} is smaller than the respective mass m_z^{l} of the longitudinal one. Accordingly, the density of states in oblique subbands, which is proportional to 3 $(m_x^{ob}m_y^{ob})^{1/2}$, is higher than in longitudinal one, concretely in the considered structures almost by one order of magnitude. As a result, in spite of the fact that the first oblique subband is significantly higher than the longitudinal one, their populations at considered carrier concentrations are of the same order. The coefficient of thermal conductivity k^e is defined at zero electrical current. The heat current in such conditions is connected with the difference of energies of two equal currents of electrons moving along ∇T and in opposite direction. In the bulk and in (100) QW the

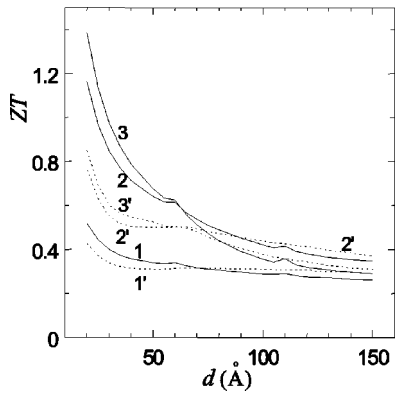

FIG. 4. Thermoelectric figure of merit ZT of $PbTe/Pb_{1-x}Eu_xTe$ quantum well as function of well width d for (100) oriented QW (curves 1, 2, 3) and for (111) ones (curves $1'$, $2'$, $3'$). Curves 1 and $1'$ are for $n=10^{18}$ cm^{-3}, 2 and $2'$ for $n=5\times10^{18}$ cm^{-3}, 3 and $3'$ for $n=10^{19}$ cm^{-3}.

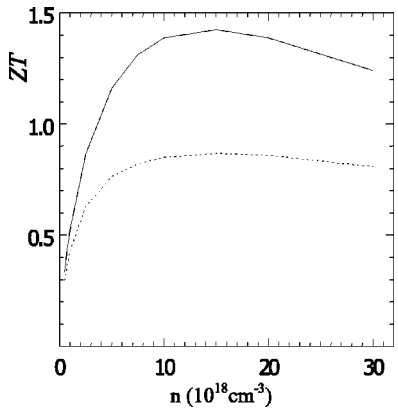

FIG. 5. Figure of merit ZT of $PbTe/Pb_{1-x}Eu_xTe$ quantum well as a function of carrier density n for (100) (solid line) and (111) QW's (dotted line).

number of carriers with high energy is exponentially small and k^e is small, too. In (111) QW's, due to presence of longitudinal and oblique subbands with approximately equal populations, electrons of these subbands create currents in opposite directions. And each such pairs of electrons carry an additional energy $\Delta E_{\alpha\beta}\sim E_\alpha^{ob}-E_\beta^l$, if Fermi energy is smaller than E_β^l, or $\Delta E_{\alpha\beta}\sim E_\alpha^{ob}-\mu$, if $\mu>E_\beta^l$. As a consequence, the thermal conductivity k_{111}^e and Lorentz number L_{111} strongly increase and achieve their maximum values at small d, when ΔE_{11} is greater. With increasing d the longitudinal and oblique subbands approach each other, $\Delta E_{\alpha\beta}$ decreases, and k_{111}^e and L_{111} decrease, too. The nonmonotonic behavior of k_{111}^e and L_{111} is caused, as in (100) case, by the appearance of new subbands in the well. But in (111) QW the number of subbands is much greater, their populations and, accordingly, the contributions to transport coefficients are smaller than in (100) case. The nonmonotonic behavior becomes less pronounced.

The effect of carrier density n increase on Lorentz number L_{111} is different at small and at large well width. At small d the increase of n leads to the decrease of L_{111} because the energies $\Delta E_{\alpha\beta}$ transported by carries decrease. At large d the carriers of the first subbands become degenerate and L_{111} increases with increasing n.

In thick QW's the values of k^e and L slightly depend on QW orientation and at very large d tend to their bulk values. At $d=150$ Å the thermal conductivity is smaller by 20% than k_{bulk}^e, calculated by the same method in the same approximations.

In Fig. 4 we show the dependencies of thermoelectric figure of merit ZT on well width for (100) and (111) QW's at different carrier concentrations. The values of ZT are greater than in the bulk and grow with the decrease of well width. Such behavior of ZT is connected with the effect of density of states increase.[1] Partially this effect is compensated by increasing scattering rate in the quasi-two-dimensional system. The latter is more pronounced at strong confinement ($U\to\infty$), when the whole carrier wave function is localized into the well. In the case of scattering on acoustic phonons the relaxation time strongly decreases with decreasing d and becomes proportional to the well width d. A complete compensation of d dependence in σ, S, k^e, and ZT takes place,[16,17] and the maximum value of ZT will be the same as in the bulk. In the case of scattering on LO phonons the relaxation time τ^{LO} decreases with decreasing d too, however, less sharply and τ^{LO} remains finite in the limit $d\to0$. As a result the optimal value of ZT increases even at $U\to\infty$. When U lowers, the wave functions become extended, the form factor in Eq. (7) and the scattering rate diminish. The complete compensation of d dependence in σ, S, and k^e does not take place and ZT increases in comparison with the case when $U\to\infty$ for both scattering mechanisms. Note, also, that when the wave function penetration into the barriers is significant, an additional strong carrier scattering on alloy disorder arises, which should be taken into consideration. As is seen from Fig. 4, the thermoelectric figure of merit is higher in (100) QW's. Although the conductivity σ_{100} is lower than σ_{111}, the enhancement of Seebeck coefficient and the decrease of thermal conductivity provide higher values of ZT (effect of valley degeneracy preservation). At large d the thermoelectric figure of merit weakly depends on QW orientation and its maximum value of $ZT\approx0.4$ is achieved at carrier concentrations $n\sim5\times10^{18}$ cm^{-3}, as in the bulk. For small d the optimal n is higher. The dependencies of ZT on electron density for $d=20$ Å are shown in Fig. 5. For both QW orientations the maximum is achieved at $n=1.5\times10^{19}$ cm^{-3}. Calculated values of the figure of merit $(ZT)^{\text{cal}}$ for thin (111) QW's agree very well with experimental results.[12] At $d\sim20$ Å in the range of concentrations $n=5\times10^{18}-5\times10^{19}$ cm^{-3} $(ZT)^{\text{cal}}=0.76-0.87$ are only a little higher than the measured ones, $(ZT)^{\text{expt}}=0.71-0.78$ in most of samples with these parameters. For thicker QW's with $d\sim40$ Å the agreement between theory and experiment is worse. Calculated ZT are two times higher than experimental values. But in very wide QW's the theory describes the experimental situation rather well.

IV. CONCLUSIONS

We present a comprehensive theoretical investigation of the electronic thermal conductivity k^e and Lorentz number L

in *n*-type PbTe/$Pb_{1-x}Eu_xTe$ quantum wells. On the basis of our model we predict the maximum expected values of the thermoelectric figure of merit $Z_{2D}T$ and determine the optimal parameters of quantum well structure required to achieve them. The proposed model is very realistic and materials specific. It includes the effect of energy band nonparabolicity, the anisotropy of carrier dispersion law, the multivalley character of the constituent bulk materials, as well the recently revised material parameters for the given system. The scattering on both acoustic and optical phonons is taken into consideration.

It is shown that the dependencies of the electronic thermal conductivity k^e and Lorentz number L on the well width have qualitatively different character in (100) and (111) oriented quantum wells. In (100) QW's the thermal conductivity k^e_{100} and Lorentz number L_{100} slightly decrease with decreasing well thickness d. For $d \leqslant 50$ Å L_{100} remains approximately constant. In (111) oriented QW's the thermal conductivity k^e_{111} and Lorentz number L_{111} strongly increase with the thickness d decreasing below 90 Å. The latter has been attributed to the lifting of the valley degeneracy and separation of the charge carriers into two groups of longitudinal and oblique subbands with very different energies. It has been concluded that, in general, the valley degeneracy lifting, when carriers are separated into two or more groups with very different energies and approximately equal concentrations, may lead to a significant increase of the electronic thermal conductivity and of the Lorentz number (as in the case of (111) QW with $d<90$ Å). At $d<90$ Å L_{111} decreases with the increasing carrier concentration n, due to the increase of Fermi energy and the decrease of thermal energy transported by the charge carriers. For large d ($d>90$ Å) L_{111} increases with increasing n. This behavior is related to the increase of degree of carrier degeneracy. The quantitative treatment of thermoelectric figure of merit has been carried out for a wide range of well width and carrier densities. Calculated $ZT=0.87$ in (111) QW at the optimum parameters $d=20$ Å and $n=1.5\times10^{19}$ cm^{-3} is two times higher than that in bulk but lower than $ZT=1.4$ in (100) QW with the same optimum parameters. The values of ZT, calculated without the use of any fitting parameters, agree very well with available experimental data for thin QW's and with the bulk value in wide wells.

ACKNOWLEDGMENT

This work was supported by U.S. CRDF-MRDA Grant No. ME2-3010.

*Corresponding author. Email address: sur@moldovacc.md

[1] L. D. Hicks and M. S. Dresselhaus, Phys. Rev. B **47**, 12 727 (1993).
[2] L. D. Hicks, T. C. Harman, and M. S. Dresselhaus, Appl. Phys. Lett. **65**, 3230 (1993).
[3] L. D. Hicks and M. S. Dresselhaus, Phys. Rev. B **47**, 16 631 (1993).
[4] J. O. Sofo and G. D. Mahan, Appl. Phys. Lett. **65**, 2690 (1994).
[5] P. J. Lin-Chung and T. L. Reinecke, Phys. Rev. B **51**, 13 244 (1995).
[6] D. A. Broido and T. L. Reinecke, Phys. Rev. B **51**, 13797 (1995).
[7] A. Balandin and K. L. Wang, J. Appl. Phys. **84**, 6149 (1998); Phys. Rev. B **58**, 1544 (1998).
[8] T. C. Harman, P. J. Taylor, M. P. Walsh, and B. E. La Forge, Science **297**, 2229 (2002).
[9] A. A. Balandin and O. L. Lazarenkova, Appl. Phys. Lett. **82**, 415 (2003).
[10] A. Balandin, A. Khitum, J. L. Liu, K. L. Wang, T. Borca-Tasciuc, and G. Chen, in *Proceeding of the 18th International Conference on Termoelectrics, Baltimore, USA* (IEEE, Piscataway, NJ, 2000), p. 189.
[11] L. D. Hicks, T. C. Harman, X. Sun, and M. S. Dresselhaus, Phys. Rev. B **53**, 10 493 (1996).
[12] T. C. Harman, D. L. Spears, and M. J. Manfra, J. Electron. Mater. **25**, 1121 (1996).
[13] D. A. Broido and T. L. Reinecke, Appl. Phys. Lett. **70**, 2834 (1997).
[14] T. Koga, T. C. Harman, S. B. Cronin, and M. S. Dresselhaus, Phys. Rev. B **60**, 14 286 (1999).
[15] A. Casian, I. Sur, H. Scherrer, and Z. Dashevsky, Phys. Rev. B **61**, 15 965 (2000).
[16] D. A. Broido and T. L. Reinecke, Phys. Rev. B **64**, 045324 (2001).
[17] D. A. Pshenay-Severin and Yu. I. Ravich, Semiconductors **36**, 908 (2002).
[18] H. Beyer, J. Nurnus, H. Bottner, A. Lambrecht, T. Roch, and G. Bauer, Appl. Phys. Lett. **80**, 1216 (2002).
[19] T. C. Harman, P. J. Taylor, D. L. Spears, and M. P. Walsh, J. Electron. Mater. **29**, L1 (2000).
[20] T. Koga, S. B. Cronin, M. S. Dresselhaus, J. L. Lui, and K. L. Wang, Appl. Phys. Lett. **77**, 1490 (2000).
[21] R. Venkatasubramanian, E. Siivola, T. Colpitts, and B. O'Quinn, Nature (London) **413**, 597 (2001).
[22] S. Yuan, H. Krenn, G. Springholz, Y. Ueta, G. Bauer, and P. J. McCann, Phys. Rev. B **55**, 4607 (1997).
[23] E. de Andrada e Silva, Phys. Rev. B **60**, 8859 (1999).
[24] G. Bastard, J. A. Brum, and R. Ferreira, Solid State Phys., Adv. Res. Appl. **44**, 229 (1991).
[25] T. Ando, A. B. Fowler, and F. Stern, Rev. Mod. Phys. **54**, 437 (1982).
[26] G. Nimtz and B. Schlicht, *Narrow-Gap Semiconductors* (Springer-Verlag, Berlin, 1982), pp. 1–117.
[27] Y. M. Lin, X. Sun, and M. S. Dresselhaus, Phys. Rev. B **62**, 4610 (2000).
[28] G. D. Mahan and J. O. Soto, Proc. Natl. Acad. Sci. U.S.A. **93**, 7436 (1996).
[29] D. L. Rode, Phys. Rev. B **2**, 1012 (1970).
[30] Y. Tokura, Phys. Rev. B **58**, 7151 (1998).
[31] Yu. I. Ravich, B. A. Efimova, and I. A. Smirnov, *Methods of Investigation of Semiconductors Applied to Lead Chalcogenides* PbTe, PbSe, PbS (Nauka Press, Moscow, 1968).
[32] S. I. Borisenko, Semiconductors **35**, 298 (2001).